New Journal of Physics
The open-access journal for physics

Magnetization reversal and exchange bias effects in hard/soft ferromagnetic bilayers with orthogonal anisotropies

D Navas[1,2,7], J Torrejon[3], F Béron[3], C Redondo[2], F Batallan[4], B P Toperverg[5,6], A Devishvili[5], B Sierra[2], F Castaño[2], K R Pirota[3] and C A Ross[1]

[1] Materials Science and Engineering Department, MIT, 02139 Cambridge, MA, USA
[2] Departamento de Química-Física, Universidad del País Vasco, E-48940 Leioa, Vizcaya, Spain
[3] Universidade Estadual Campinas, Instituto de Fisica Gleb Wataghin, BR-13083970 Campinas, SP, Brazil
[4] Instituto de Ciencia de Materiales de Madrid, CSIC, Cantoblanco, E-28049 Madrid, Spain
[5] Department of Physics, Ruhr-Universitat Bochum, D-44780 Bochum, Germany
[6] Theory Division, Petersburg Nuclear Physics Institute, Gatchina, 188300 St Petersburg, Russia
E-mail: davidnavasotero@gmail.com

New Journal of Physics **14** (2012) 113001 (21pp)
Received 6 June 2012
Published 2 November 2012
Online at http://www.njp.org/
doi:10.1088/1367-2630/14/11/113001

Abstract. The magnetization reversal processes are discussed for exchange-coupled ferromagnetic hard/soft bilayers made from $Co_{0.66}Cr_{0.22}Pt_{0.12}$ (10 and 20 nm)/Ni (from 0 to 40 nm) films with out-of-plane and in-plane magnetic easy axes respectively, based on room temperature hysteresis loops and first-order reversal curve analysis. On increasing the Ni layer thicknesses, the easy axis of the bilayer reorients from out-of-plane to in-plane. An exchange bias effect,

[7] Author to whom any correspondence should be addressed.

consisting of a shift of the in-plane minor hysteresis loops along the field axis, was observed at room temperature after in-plane saturation. This effect was associated with specific ferromagnetic domain configurations experimentally determined by polarized neutron reflectivity. On the other hand, perpendicular exchange bias effect was revealed from the out-of-plane hysteresis loops and it was attributed to residual domains in the magnetically hard layer.

Contents

1. Introduction

Ferromagnetic (FM) thin films with strong out-of-plane magnetic anisotropy have been widely studied for perpendicular magnetic recording media applications [1, 2]. For this purpose, perpendicular anisotropy systems can be designed with high thermal stability to avoid superparamagnetic behavior [3] and with good writeability [1], but this may raise the switching field above that which can be produced by currently available write heads. The use of tilted media, where the easy magnetization axis points at 45° to the film plane, has been proposed to reduce the switching field [4, 5], but the implementation of this method is complex.

Considerable research has therefore been done on multilayer magnetic films where exchange coupling between dissimilar phases can be used to tailor the magnetic response. For example, thermally assisted recording media was suggested as a possibility to overcome the writing problem [6], by coupling a hard layer to a layer such as FeRh with strongly temperature-dependent magnetic properties [7–10].

Perpendicular exchange coupled composite or exchange spring media have recently been introduced as candidate systems in which the magnetic response can be controlled without the necessity for thermal cycling [11–16]. Perpendicular exchange spring systems consist of exchange-coupled hard and soft magnetic layers with respectively out-of-plane and in-plane easy magnetization axes. While the magnetically hard film provides thermal stability, the soft layer reduces the reversal field. When an external magnetic field is applied, the soft layer reverses first which creates an additional effective field applied to the hard phase through exchange coupling, lowering the switching field of the whole system. Hard layers with high coercive fields and magnetocrystalline anisotropy constant on the order of $7 \times 10^6\,\mathrm{J\,m^{-3}}$, such as FePt, CoPd and CoPt, and soft layers of materials with low magnetocrystalline anisotropy and large saturation magnetization such as FeNi, have been suggested for exchange spring media, i.e. the effective anisotropy energies of the component layers are highly dissimilar [11–13].

FePt and FeNi [17], FePt and Fe_3Pt [12], FePt and Fe [16, 18, 19], FePt and FeAu [20], Pt/Co multilayers and FeNi [21], CoPtNi and Ni oxides [22], and CoPt-SiO_2 and Co-SiO_2 [23] composites are some examples which have been experimentally studied.

Another phenomenon of interest in coupled FM layer systems is the exchange bias effect observed between two ferromagnets with perpendicular anisotropies at room temperature without any field cooling procedure. Usually, exchange bias results from the interfacial exchange interaction between a FM and an AFM (antiferromagnetic) material [24–27] and is manifested by a shift H_{EB} of the FM hysteresis loop along the magnetic field axis after field-cooling through the Néel temperature of the AFM. An induced exchange bias behavior has also been observed in systems with two coupled FM materials such as a Pt/Co multilayer and a NiFe thin film [21, 28, 29]. A shift (H_{EB}) of the in-plane room temperature hysteresis loops of the NiFe layer was observed when the loops were measured after an in-plane saturation of the whole system. This effect was explained as a result of the interplay between out-of-plane and in-plane anisotropies of the Pt/Co multilayer and NiFe thin film, respectively. As the out-of-plane magnetization of each domain in the Pt/Co progressively tilts toward the in-plane direction, closure domains are created in the region close to the interface [30, 31]. Closure domains at the interlayer were suggested by Sort *et al* [28] and predicted by two-dimensional micromagnetic simulations [21, 32]. When the system approaches in-plane saturation, the closure domains in the hard layer, oriented parallel and anti-parallel to the external field, change their respective sizes, and the net in-plane magnetic moment from the uncompensated closure domains induces an exchange bias effect on the minor hysteresis loop of the soft phase [21, 28, 29]. Recently, micromagnetic simulations [33] showed the formation of vortex cores in the Bloch domain walls separating the upwards and downwards magnetization domains in the Pt/Co multilayer. Bollero *et al* [33] suggested that the contribution of the exchange coupling between the magnetization of the NiFe layer and the magnetization of the vortex cores (aligned parallel to the in-plane applied field) is responsible for the shift (H_{EB}) of the in-plane NiFe layer hysteresis loops.

In contrast, no shifts along the field axis were observed when the external magnetic field was applied out-of-plane [28]. Recently, simultaneous in- and out-of-plane exchange bias has been obtained by coupling a FM with in-plane anisotropy and a FM with out-of-plane anisotropy to the same AFM layer such as Co/NiO/Co–Pt [34] and NiFe/IrMn/Co–Pt [35] stacks.

In this work, we examined bilayers composed of two materials (CoCrPt and Ni) which present anisotropies of similar magnitudes but orthogonal directions, out-of-plane in the case of CoCrPt and in-plane for Ni. We selected a Co-based alloy ($Co_{0.66}Cr_{0.22}Pt_{0.12}$) as the hard material with uniaxial magnetocrystalline anisotropy [36, 37], which can be oriented out-of-plane by epitaxial growth onto a Ti (0001) underlayer. This alloy has been extensively studied for hard-disk data storage applications [38, 39]. We completed the exchange-coupled system with a Ni film as the soft layer. Due to its low magnetocrystalline anisotropy, shape anisotropy controls its magnetic properties. The soft layer thickness was varied from 0 to 40 nm, keeping the hard layer thickness at 10 or 20 nm. A reorientation of the bilayer magnetization configuration from out-of-plane to in-plane occurs as the Ni film thickness increases (shown in section 3.1). Room temperature hysteresis loops and first order reversal curve (FORC) analysis [40–43] were performed to determine the magnetization reversal process of the exchange-coupled systems as a function of layer thicknesses (section 3.2). We also examined the in-plane exchange bias effect for the Ni layer after saturating the CoCrPt/Ni composites (section 3.3). In prior work [21, 28, 29], where in-plane exchange bias effects were studied, composites with thinner in-plane soft layers (up to 5 nm thick) were examined. In this paper, the magnetization reversal

processes and exchange bias effects are reported for composites where the Ni layer thickness was varied in a broader range (between 0 and 40 nm). Conclusions on the nature of the exchange bias effect, deduced from the hysteresis loops and the FORC analysis, are complemented by the results on the depth resolved magnetometry reported in section 3.4. The magnetization distribution across the CoCrPt/Ni bi-layer is provided by polarized neutron reflectometry (PNR). This method is capable [44–46] of probing magnetic states of CoCrPt layer deeply buried under the thick Ni layer. In this case, other domain imaging methods, such as magnetic force microscopy [47], photoemission electron microscopy [48], transmission x-ray microscopy [49], or circular dichroism in x-ray resonant magnetic scattering [50] are inapplicable. PNR analysis at low field showed that, while the 40 nm thick Ni layer remains close to saturation, the in-plane magnetization of the CoCrPt phase linearly decays through the layer thickness. This magnetization profile supports the existence of a domain configuration responsible for the exchange bias effect.

In section 3.5, we reported on the observation of out-of-plane exchange bias induced by applying a saturating field perpendicular to the film surface. The perpendicular exchange bias effect was interpreted within a model of residual domains in CoCrPt layer [49].

2. Experimental methods

A 5 nm Ti seed layer, a 10 or 20 nm thick Co66 at%/Cr22 at%/Pt 12 at% (CoCrPt) film, then a Ni film with thicknesses from 0 to 40 nm and finally a 3 nm Ti capping layer were deposited sequentially on (100) Si wafers with native oxide by rf sputtering at room temperature. The Ar (99.999% pure) sputtering gas pressure was 2 mTorr, with a base pressure below 2×10^{-8} Torr, and the rf power was 300 W for 5 cm diameter targets [51, 52]. The deposition rates were 1.9 Å s^{-1} for CoCrPt, 1.4 Å s^{-1} for Ni and 0.8 Å s^{-1} for Ti. For clarity, the samples are named in the following sections as CoCrPtX/NiY where X and Y represent the thicknesses in nm of the CoCrPt and Ni films, respectively.

In the sputtering system, the thickness of the deposited layer is homogenous over the central area ($\approx 2 \times 2\,\mathrm{cm}^2$) of the sample and is reduced at larger radii. The hysteresis loops and FORC analysis used samples with areas of $5 \times 5\,\mathrm{mm}^2$ cut from the center of the sample where the final layer thicknesses is consistent with the nominal thickness values. However, polarized neutron measurements require larger areas and we measured samples with areas as large as $3 \times 3\,\mathrm{cm}^2$. The average film thickness of the large samples is expected to be lower than the nominal thickness.

Room temperature magnetic characterization was performed by measuring the hysteresis loops in a vibrating sample magnetometer (VSM, ADE model 1660) and FORCs were measured with a commercial Lakeshore magnetometer (model 7400). FORC measurements consist of several minor hysteresis loops, beginning at different reversal fields H_r and going back to positive saturation. The FORC distribution ρ represents the statistical distribution of the system of hysterons. It can be calculated through a second-order mixed derivative of magnetization M with respect to applied field H and H_r [53],

$$\rho\,(H, H_r) = -\frac{1}{2}\frac{\partial^2 M}{\partial H\,\partial H_r} \quad (H \geqslant H_r). \tag{1}$$

This derivative eliminates the purely reversible components of the magnetization ($\rho = 0$) [54]. Thus, any non-zero ρ corresponds to irreversible switching processes [40]. The results are

presented in the Preisach plane using the interaction field axis, $H_u = -(H + H_r)/2$, and the critical field axis, $H_{cr} = (H - H_r)/2$ (written as H_c in the FORC diagrams). The precision of the FORC diagram is governed by the magnetic field and reversal field steps, ΔH and ΔH_r, respectively. In this work, we selected a saturation field H_s of 5 kOe, $\Delta H = 5$–25 Oe and $\Delta H_r = 5$–50 Oe, based on the major hysteresis loops.

We induced exchange bias effects in the CoCrPt/Ni bilayer through the following procedure: after saturation (15 kOe), we measured a minor loop with a maximum applied field (H_{max}) large enough to saturate one of the phases but insufficient to saturate the other one. Minor loops were measured with H_{max} values of 750 Oe, 1 kOe and 1.25 kOe after both positive and negative saturation of the composite, in order to check the symmetry of this phenomenon. This procedure was carried out with fields along both the in- and out-of-plane directions, in order to determine H_{EB} fields of the Ni and CoCrPt layers respectively.

Polarized neutron scattering experiments were carried out with the Super ADAM reflectometer (www.ill.eu/instruments-support/instruments-groups/instruments/superadam/) at the Institut Laue–Langevin, Grenoble (France). The measurements were performed with fixed neutron wavelengths of $\lambda = 0.441$ nm and the polarization efficiency was around 95%. The external magnetic field (up to 7 kOe) was applied in-plane, parallel to the neutron polarization and perpendicular to the scattering plane. For specular reflectivity measurements, non-spin-flip (NSF) reflectivities as well as neutrons with flipped polarization after reflection were analyzed.

3. Results and discussion

3.1. Hysteresis loops and anisotropy

Single-layer CoCrPt films show out-of-plane easy magnetization direction because the anisotropy energy is primarily controlled by the magnetocrystalline anisotropy term (figure 1(a)). Magnetic measurements and x-ray diffractometry of similar CoCrPt films [36, 52, 55] indicate that the crystallographic *c*-axis and the easy magnetization axis are oriented out of plane. Along the out-of-plane direction, no magnetization reversal is observed until the external magnetic field reaches the 'depinning field' (H_{Dp}). Then, a sharp magnetization drop occurs which is associated with an avalanche-like growth of reverse domains in the film. While the hysteresis loop shape is almost square for the 10 nm thick film (not shown here), the 20 nm thick film (figure 1(a)) shows a slow approach to saturation which is attributed to the existence of small bubble domains that are magnetostatically stabilized by the surrounding regions. A linear or almost linear hard axis behavior was exhibited by single layer CoCrPt films when the magnetic field was applied in-plane. In contrast, Ni thin films show a square loop for an in-plane field associated with domain wall nucleation and propagation processes (figure 1(b)), while the out of plane direction is a hard axis. For comparison, out-of-plane (figure 1(c)) and in-plane (figure 1(d)) hysteresis loops of several CoCrPt20/NiY composites are also shown. The shape of the composite loops cannot be explained by a simple superposition of the individual layers, indicating the existence of magnetic interactions between the phases.

We first consider the effective magnetic anisotropy energy (K^{eff}) in the composite films. An estimate of K^{eff} for each film was obtained from the hysteresis loop, using the following approximation:

$$K^{eff} = \int_0^{M_S} (H - H_c)_{In\_Plane}\, dM - \int_0^{M_S} (H - H_c)_{Out\_Plane}\, dM, \qquad (2)$$

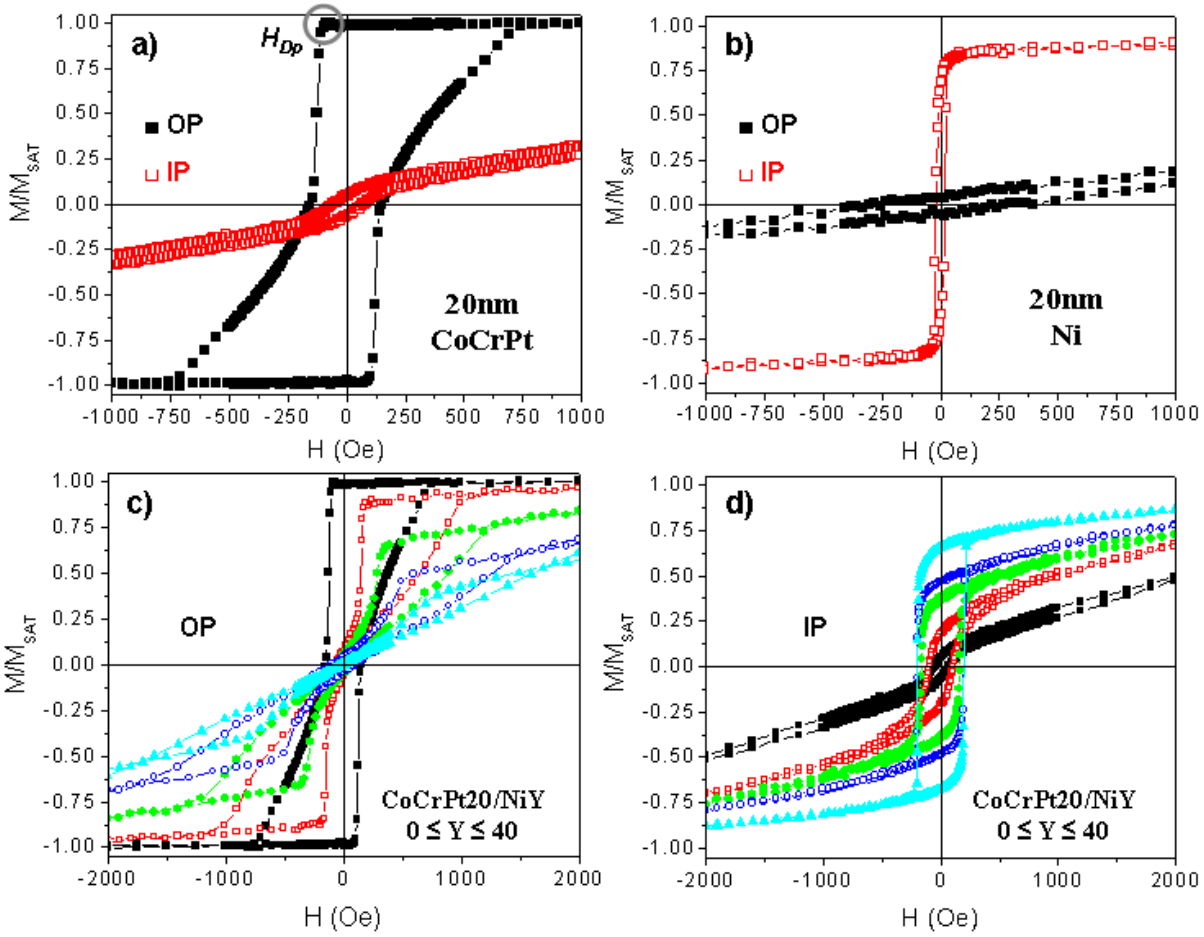

Figure 1. In-plane (□) and out-of-plane (■) hysteresis loops of (a) a 20 nm thick CoCrPt film and (b) a 20 nm thick Ni film. (c) Out-of-plane and (d) in-plane hysteresis loops of CoCrPt20/NiY composites with $Y = 0$ nm (■), 5 nm (□), 10 nm (•), 20 nm (○) and 40 nm (▲).

where M_S is the saturation magnetization and H_c the coercivity. Positive values ($K^{eff} > 0$) favor perpendicular magnetization and negative values ($K^{eff} < 0$) favor in-plane magnetization. The competition between the different anisotropy terms in CoCrPtX/NiY bilayers is the origin of the reorientation of the easy direction from out-of-plane to in-plane when the Ni thickness is increased. This reorientation occurs around $t_{Ni} = 5$ and 10 nm for $t_{CoCrPt} = 10$ and 20 nm respectively (figure 2).

Under the assumption that both layers, with saturation magnetization $M_S^{hard(soft)}$ and film thicknesses $l^{hard(soft)}$ of the hard (soft) layer, remain magnetically uniform and the layers are exchange coupled, the bilayer structure can be described with an average magnetization

$$M_{S-T}^{eff} = \left(\left(M_S^{hard} \times l^{hard}\right) + \left(M_S^{soft} \times l^{soft}\right)\right)/\left(l^{hard} + l^{soft}\right) \tag{3}$$

and anisotropy constant [56, 57]

$$K_T^{eff} = \left(\left(K^{eff\ hard} \times l^{hard}\right) + \left(K^{eff\ soft} \times l^{soft}\right)\right)/\left(l^{hard} + l^{soft}\right) \tag{4}$$

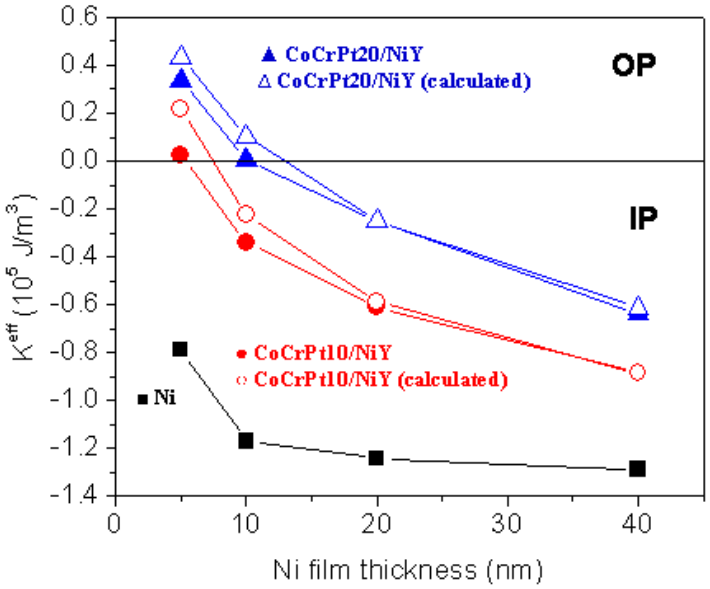

Figure 2. Experimental values from equation (2) for the effective anisotropy energy of Ni (■), $t_{CoCrPt} = 10$ nm (●) and $t_{CoCrPt} = 20$ nm (▲) composites and predicted values from equation (4) for $t_{CoCrPt} = 10$ nm (○) and $t_{CoCrPt} = 20$ nm (△) composites as a function of the Ni film thicknesses.

i.e. the bilayer structure exhibits the same magnetic behavior as a single layer structure with M_{S-T}^{eff} and K_T^{eff}. The model (equation (4)) predicts transitions from out-of-plane to in-plane for Ni film thicknesses of 7.5 and 13 nm for $t_{CoCrPt} = 10$ and 20 nm respectively, slightly higher than the experimental measurements (figure 2). Although micromagnetic simulations show that the assumption of uniform reversal of both hard and soft layers is not valid for most exchange coupled composite structures [13], the results for the CoCrPtX/NiY composites fit quite well with this behavior when the easy magnetization axis lies in-plane, i.e. uniform reversal of both layers is suggested for systems with $t_{Ni} \geqslant 20$ nm. Composites with thinner Ni films show discrepancies between the experimental and predicted effective anisotropy energy values which are associated with inhomogeneous reversal processes of the soft and hard phases.

3.2. First order reversal curves

The FORC technique was employed to examine the reversal process in greater detail. Figure 3 shows the evolution of the FORC results of the 40 nm thick Ni film and two composites (CoCrPt10/Ni40 and CoCrPt20/Ni40) when the external magnetic field was applied in-plane. For the single Ni film, the obtained circular FORC distribution is in agreement with a domain wall nucleation-propagation process (figure 3(a)). Although the bilayers (figures 3(b) and (c)) present a similar behavior, there is a curve in the FORC distributions and a positive shift along the H_u-axis, suggesting that the CoCrPt layer alters the Ni reversal process.

Major hysteresis loops give averaged properties such as coercivity and reduced remanence which represent the behavior of the whole bilayer system. On the other hand, characteristics extracted from FORC results, such as the H_{cr} where the FORC distribution is maximum (denoted H_{crmax}), are related to local properties, e.g. the fields at which irreversible events

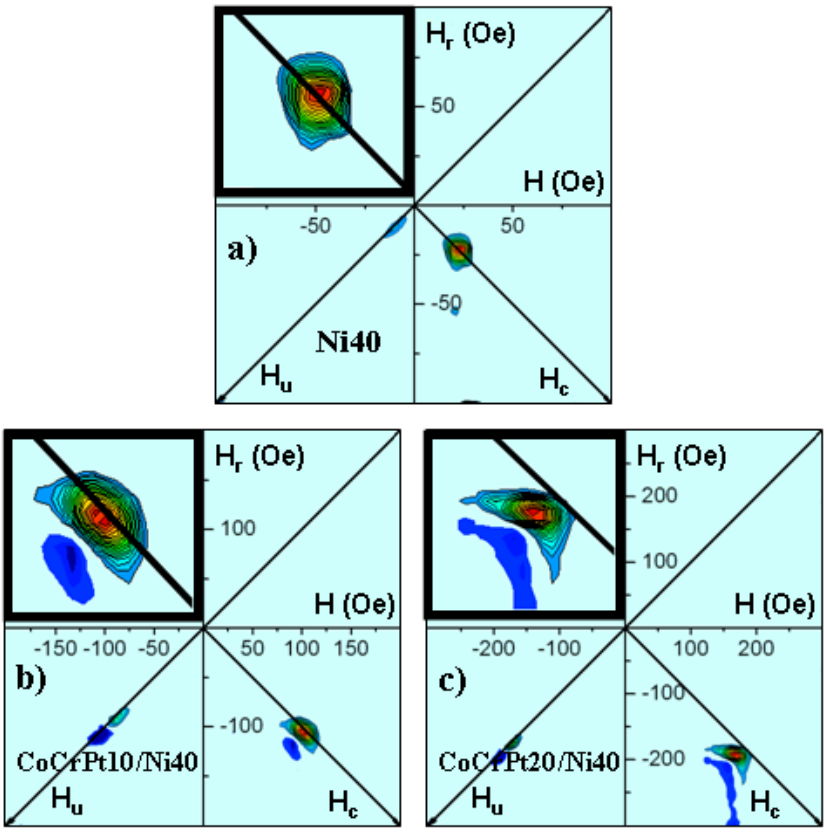

Figure 3. In-plane FORC results of 40 nm thick Ni layer (a), CoCrPt10/Ni40 (b) and CoCrPt20/Ni40 (c) composites. The boxed insets show a magnified view of part of the lower right quadrant (irreversible features). The FORC diagonal axes are critical field H_{cr} (written as H_c in the plots) and interaction field H_u. The color scale of the FORC diagrams ranges from light blue to red for $\rho \geqslant 0$ and from light blue to black for $\rho \leqslant 0$.

occur. In-plane VSM coercivities and FORC Ni layer switching fields H_{crmax} are summarized in figure 4(a) as a function of the Ni film thickness. Both the coercivity measured from VSM (H_c) and the Ni layer switching fields from FORC (H_{crmax}) of the composites present similar trends compared to the single Ni layers (figure 4(a)). While the VSM coercivity H_c is identical to the local Ni switching field H_{crmax} for single layer Ni films (as expected), it is larger in the composite films due to the coupling between the films. The difference, more or less constant with the Ni thickness, increases with the CoCrPt film thicknesses from 7.8 to 27.7 Oe for $t_{CoCrPt} = 10$ and 20 nm, respectively. Therefore, the switching field H_{crmax} of a soft material with in-plane easy axis can be tailored by adding a well-coupled hard layer with out-of-plane easy magnetization axis.

Comparing the reduced remanences obtained from the VSM data, we observe that M_R/M_{SAT} of the composites exhibits the same increasing tendency as the single layer Ni film (full symbols in figure 4(b)). Figure 4(b) also shows the reduced remanence of the composites calculated on the basis that the two layers are fully decoupled (open symbols in figure 4(b)). The fully decoupled values were obtained from summing the hysteresis loops of the CoCrPt single

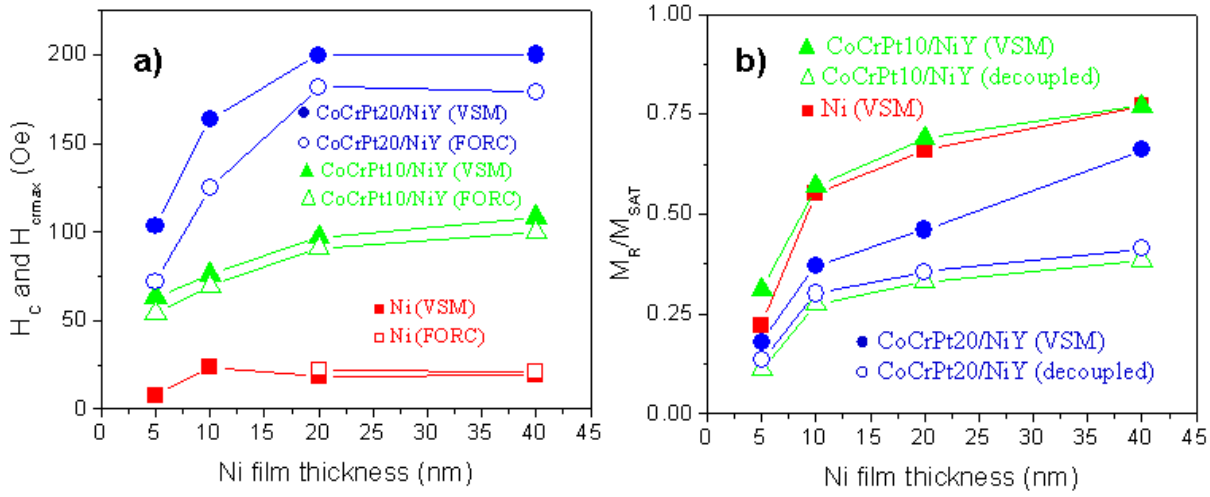

Figure 4. (a) Coercivity from VSM (full symbols) and Ni layer switching fields (H_{crmax}) from FORC (open symbols) of Ni (■) and composites with 10 (▲) and 20 (●) nm thick CoCrPt films as a function of the Ni film thicknesses. (b) Reduced remanence of Ni (■) and composites with 10 (▲) and 20 (●) nm thick CoCrPt films as a function of the Ni film thicknesses obtained from the VSM (full symbols). Reduced remanence of composites which are magnetically fully decoupled (open symbols).

layer and the Ni single layer. As $M_{\mathrm{R}}/M_{\mathrm{SAT}}$ values for the composites (full symbols in figure 4(b)) are larger than the expected values for a fully decoupled system (open symbols in figure 4(b)) and even larger than the Ni values in the $t_{\mathrm{CoCrPt}} = 10$ nm case, an extra contribution to the in-plane magnetization is present. Thus, we propose that the CoCrPt magnetization partially rotates toward the in-plane direction due to the interfacial exchange coupling with the Ni film [21, 28]. This is consistent with the PNR measurements discussed below.

We now discuss out-of-plane FORC results. The behavior of perpendicular exchange spring systems, when the external magnetic field is applied out-of-plane, can be summarized by the following steps [11–16]:

(i) first of all, the system is fully saturated at large out-of-plane fields;

(ii) when the external magnetic field is reduced and a 'nucleation field' (H_{N}) is reached, the magnetization direction in the soft material starts to rotate from out-of-plane to in-plane in a reversible way. This leads to domain wall nucleation and propagation in the soft phase. Finally, the domain wall is pinned at the soft/hard interface;

(iii) the magnetization reversal of the hard layer is completed by a sharp jump at the 'depinning field' (H_{Dp}). This last step has been associated with the domain wall depinning and propagating through the hard phase of the system, which is an irreversible process. Thus the FORC would show a single peak at H_{Dp}. At sufficient reverse field, the soft layer is fully reversed.

Figure 5 shows the out-of-plane hysteresis loops and FORC results of a 20 nm thick CoCrPt film and two composites (CoCrPt20/Ni5 and CoCrPt20/Ni20). The out-of-plane hysteresis loops, especially those for composites with $t_{\mathrm{CoCrPt}} = 20$ nm (figures 5(b) and (c)),

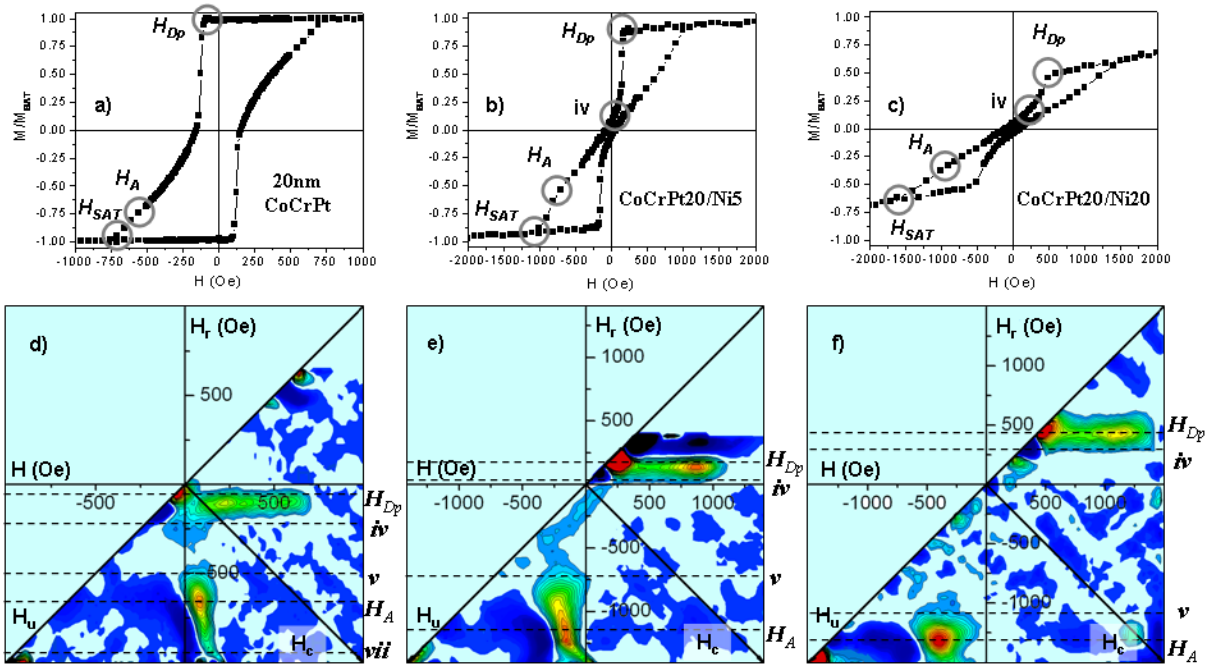

Figure 5. Out-of-plane hysteresis loops ((a)–(c)) and FORC results ((d)–(f)) of 20 nm thick CoCrPt film ((a) and (d)) and CoCrPt20Ni5 ((b) and (e)) and CoCrPt20Ni20 composites ((c) and (f)). Gray circles in the hysteresis loops and dashed lines in the FORC diagrams show the different magnetization reversal steps. The FORC diagonal axes are critical field H_{cr} (written as H_c in the plots) and interaction field H_u.

are characteristic of magnetic thin films with perpendicular magnetic anisotropy which can have a multidomain configuration [40, 58, 59], suggesting a different reversal process from the process described above (see circles in figures 5(a)–(c)). Moreover, the out-of-plane FORC results (even in the single CoCrPt layers) present two peaks associated with irreversible processes which also confirms magnetization reversal via multiple steps [17, 40, 41] (shown by dashed lines in figures 5(d)–(f)). The first peak is associated with the depinning process, with $H_r = H_{Dp}$ (described above, step (iii)). Using the FORC analysis that Davies *et al* [40] carried out for studying the magnetization reversal of Pt/Co multilayers, the next steps are described by (see circles in figures 5(b) and (c), and dashed lines in figures 5(d)–(f)):

(iv) the hard phase breaks into a multidomain configuration after the depinning of the interface domain wall. This hypothesis is reinforced by the horizontal elongation of the H_{Dp} peak, which reflects a gradual return to saturation just after the wall depinning, instead of a sharp jump. Thus, an extended reversible region ($\rho \approx 0$) at low field (between points (iv) and (v)) is explained by expansion of the domains in the hard layer;

(v) a second irreversible process starts to occur, leading to a second peak;

(vi) this second peak, the 'annihilation field' (H_A), observed in the CoCrPt layer with or without a Ni layer, is associated with the annihilation of the domains in the CoCrPt film until it reaches saturation;

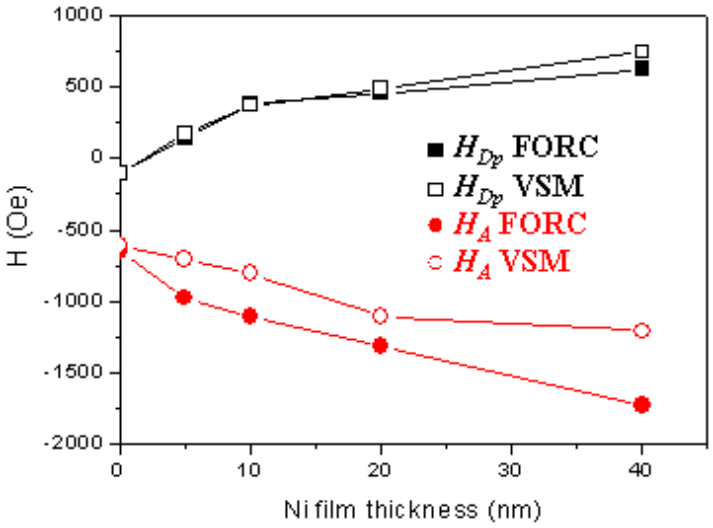

Figure 6. *Depinning* (■) and *annihilation* (•) fields of composites with 20 nm CoCrPt thick obtained from major hysteresis loops (open symbols) and FORC distributions (full symbols).

(vii) irreversible features are still observed for reverse fields $H_r < H_A$ (between points H_A and (vii)) until the CoCrPt layer is fully saturated (H_{SAT});

(viii) finally, reversible changes in the magnetization ($\rho \approx 0$) are observed until the Ni layer is fully saturated out of plane ($H_r < H(\text{vii}) = H_{SAT}$), which requires large external fields to overcome the shape anisotropy of the Ni thin film.

As the FORC technique uses a large data set in comparison to the usual major hysteresis loops, it can reveal much more detailed information about the reversal process of a system. For example, the FORC diagram of the 20 nm thick CoCrPt layer shows a reversible region (associated with the expansion and contraction of the domains) between points (iv) and (v) ($-500 < H_r < -250$ Oe). Also, FORC results show larger H_A values than the hysteresis loops (figure 6) and even the irreversible processes persist well beyond the field (H_{SAT}) at which saturation is nominally reached. This is consistent with the presence of bubble domains in the CoCrPt, even though their resulting magnetic moment becomes negligible in the hysteresis loops [17, 40]. Larger fields, such as $H_r \approx -1400$ Oe for 20 nm thick CoCrPt film, are required to fully saturate the CoCrPt.

Figure 6 shows the evolution of both *depinning* and *annihilation* fields of composites with 20 nm thick CoCrPt as a function of the Ni thickness. From both the major hysteresis loops (open symbols in figure 6) and the FORC distributions (full symbols in figure 6), one can suggest that the presence of the Ni layer seems to favor the stability of the multidomain state of the CoCrPt layer, increasing the absolute values of both H_{Dp} and H_A. Therefore, the step between both irreversible peaks (from point (iv) to (v) in figure 5) is larger when the Ni layer is thicker ($-500 < H_r < -250$ Oe for 20 nm thick CoCrPt, $-800 < H_r < +250$ Oe for CoCrPt20/Ni5 and $-1000 < H_r < +250$ Oe for CoCrPt20/Ni20). A similar tendency was observed for $t_{CoCrPt} = 10$ nm.

3.3. Exchange bias effects in CoCrPt/Ni composites in an in-plane field

In this section, we discuss the in-plane exchange bias effects in exchange-coupled FM bilayers with perpendicular anisotropies. Figure 7(a) shows an example of the in-plane minor loops of a CoCrPt20/Ni10 composite with minor loop amplitude $H_{max} = 750$ Oe, 1 kOe, 1.25 kOe and 10 kOe after a positive saturation (+15 kOe). The minor hysteresis loops were obtained starting the measurements from positive H_{max} ($+H_{max} \rightarrow -H_{max} \rightarrow +H_{max}$). Vertical shifts of the hysteresis loops along the magnetization axis are observed. As the maximum applied field in the minor loop is increased, these shifts are reduced [28]. Figure 7(b) shows the in-plane minor loops of the CoCrPt20/Ni10 composite after centering the loops along the magnetization axis with $H_{max} = 750$ Oe and 10 kOe after a positive saturation (+15 kOe). While the loop is symmetrical along the field axis for $H_{max} = 10$ kOe, the ascending branch of the minor loop performed with $H_{max} = 750$ Oe (i.e. from –750 to +750 Oe) has a lower coercivity than the descending branch, yielding a significant shift of the loop toward negative field values and a coercivity decrease. On the other hand, the minor hysteresis loops show reversed behavior [60] (figure 7(c)) when they were started from negative $H_{max} = -750$ Oe ($-H_{max} \rightarrow +H_{max} \rightarrow -H_{max}$) and after negative saturation (−15 kOe).

Finally, a symmetric minor loop (figure 7(d)) without any shift and lower coercivity is observed when the cycle was performed from a negative field, $H_{max} = -750$ Oe ($-H_{max} \rightarrow +H_{max} \rightarrow -H_{max}$) after an in-plane demagnetization process.

In contrast with these results, CoCrPt10/NiY composites with $Y > 5$ nm showed no such exchange bias effects under the same field cycling procedures.

As mentioned in the introduction, an exchange bias effect along the applied field axis in systems with two coupled ferromagnetic materials has been explained by considering the domain configurations of the two magnetic layers [21, 28, 33]. When the system is saturated in-plane and the external field is removed, an effective in-plane magnetic moment is retained from the uncompensated domains in the hard phase, favoring magnetization along the direction in which the sample was initially saturated.

The uncompensated domains produce, as a first consequence, a shift of the loops along the magnetization axis when the maximum applied field is large enough to reverse the layer with in-plane anisotropy but not enough to eliminate the hard layer domain structure [28, 60]. This magnetization offset depends on the maximum applied field and it is negligible for large enough external fields (figure 7(a)).

A second consequence is that negative (figure 7(b)) or positive (figure 7(c)) shifts of the soft layer hysteresis loop along the field axis (i.e. an in-plane exchange bias effect) [28, 60] and a coercivity reduction are observed when only the layer with in-plane anisotropy was saturated after saturating the bilayer. The measured coercivity and the in-plane exchange bias along the field axis are plotted in figures 8(a) and (b) for composites with $t_{CoCrPt} = 20$ nm.

In contrast, when the minor loop was measured after in-plane demagnetization process, the contribution to the in-plane magnetization of the hard layer domains was compensated and no shifts were observed (figure 7(d)). Moreover, the compensated domain configurations are robust enough to not be modified by applied fields favoring the reversal of the soft phase on both the ascending and descending loop branches and reducing the coercive fields (open symbols in figure 8(a)).

Because the domain configuration was artificially created, the pinning effect can be easily modified by applying sufficiently large fields. Figure 8(b) shows how the H_{EB} values are reduced

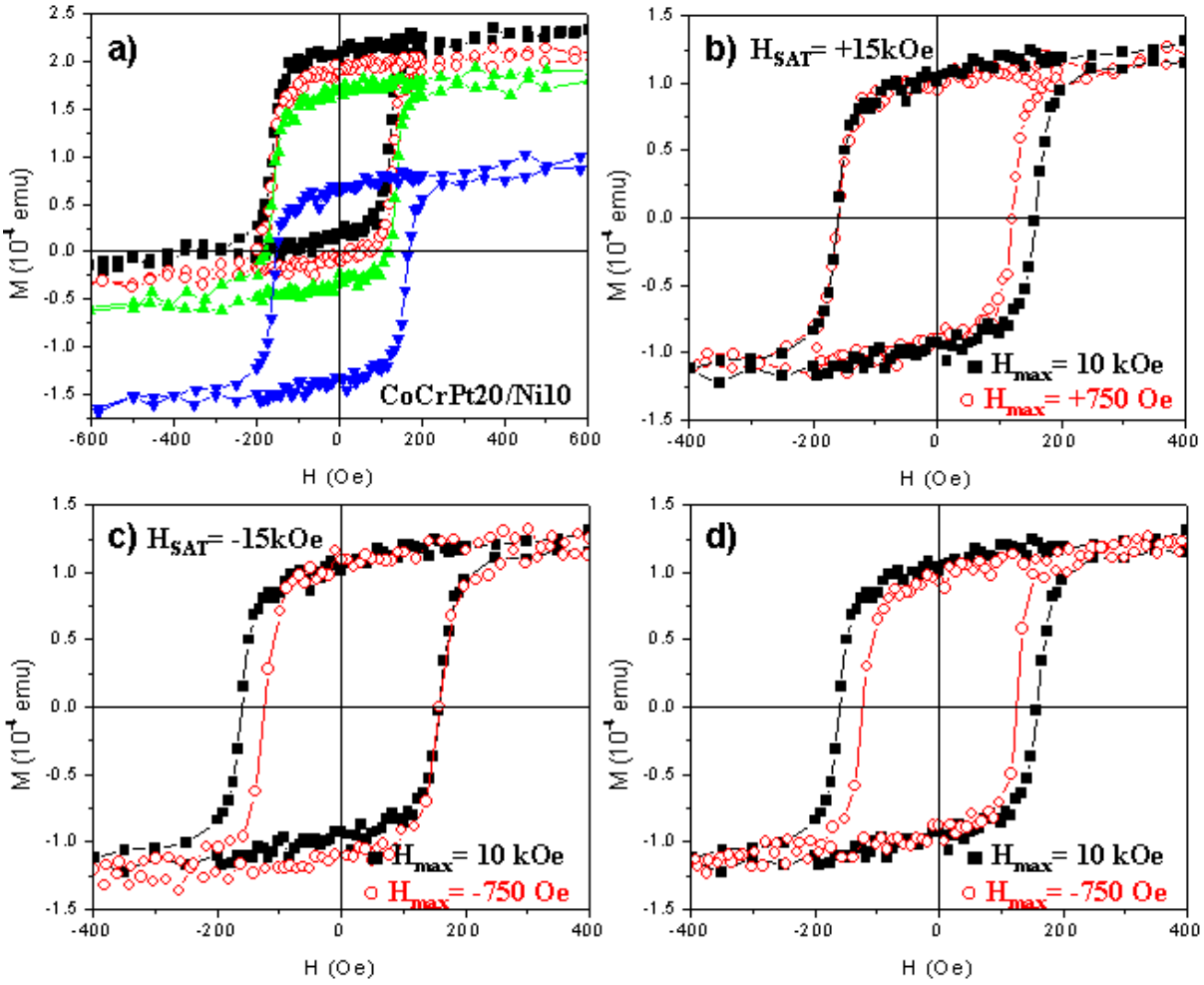

Figure 7. (a) In-plane hysteresis loops of CoCrPt20/Ni10 bilayer with +750 Oe (■), +1 kOe (○), +1.25 kOe (▲) and +10 kOe (▼) maximum external applied field after the full saturation of the system with +15 kOe. (b) In-plane hysteresis loops of CoCrPt20/Ni10 composite after centering the loops along the magnetization axis with +750 Oe (□) and +10 kOe (■) maximum external applied field after the saturation with +15 kOe; (c) with −750 Oe (□) and +10 kOe (■) maximum external applied field after saturation with −15 kOe; and (d) with −750 Oe (□) and +10 kOe (■) maximum external applied field after in-plane demagnetization process.

when the maximum applied field is increased. The H_{EB} also reduces for thicker Ni layers and the coercivity tends to a maximum value (figure 8(a)), supporting its interpretation as an interface effect.

Although no in-plane exchange bias effects were observed for CoCrPt10/NiY composites, FORC results exhibited features similar to those seen in the CoCrPt20/NiY composites, consistent with the presence of a magnetizing interaction field, but any bias effects were too small to be observed in our VSM measurements.

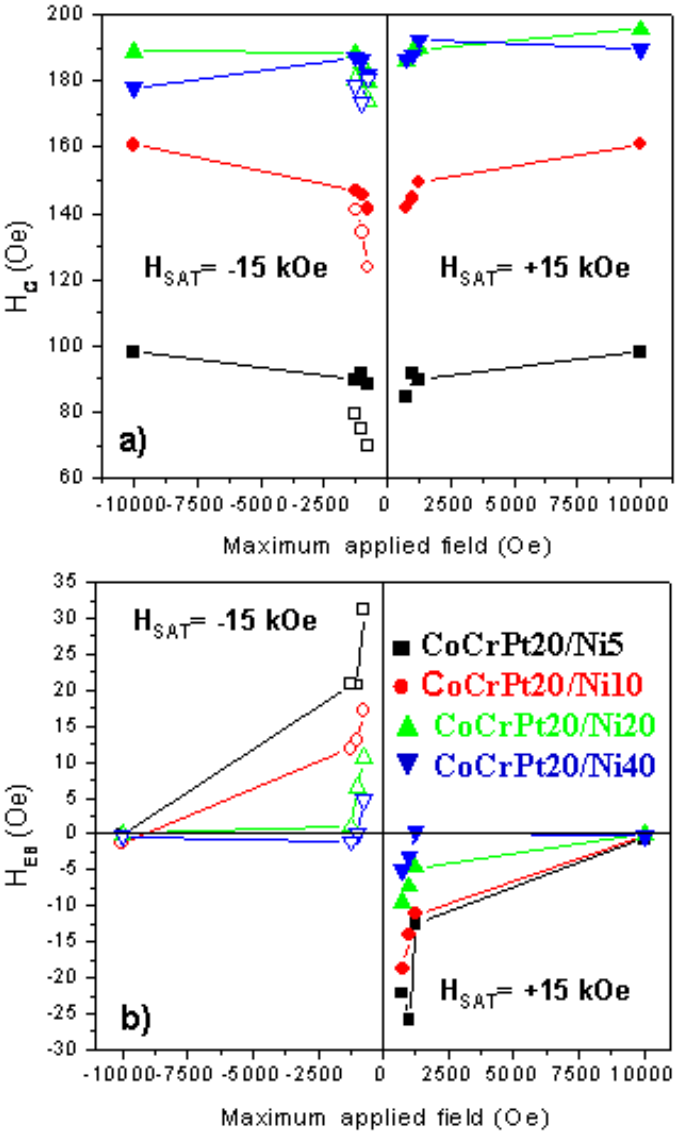

Figure 8. (a) Coercivity from VSM of the composites with 20 nm thick CoCrPt plus 5 (■), 10 (•), 20 (▲) and 40 nm (▼) Ni as a function of the maximum external applied field after the systems were saturated at +15 kOe (right panel) and −15 kOe (left panel) in plane. The open symbols show the coercivity as a function of the maximum external applied field (starting from negative values) after in-plane demagnetization process of the system. (b) Exchange bias fields of composites with 20 nm thick CoCrPt plus 5 (■), 10 (•), 20 (▲) and 40 nm (▼) Ni as a function of the maximum external applied field after the systems were saturated at +15kOe (full symbols) and −15 kOe (open symbols).

3.4. Polarized neutron reflectivity

Based on the foregoing discussion, magnetic domains at the interface provide a plausible origin for the increased remanence of the bilayer and for the exchange bias effects. In order to check

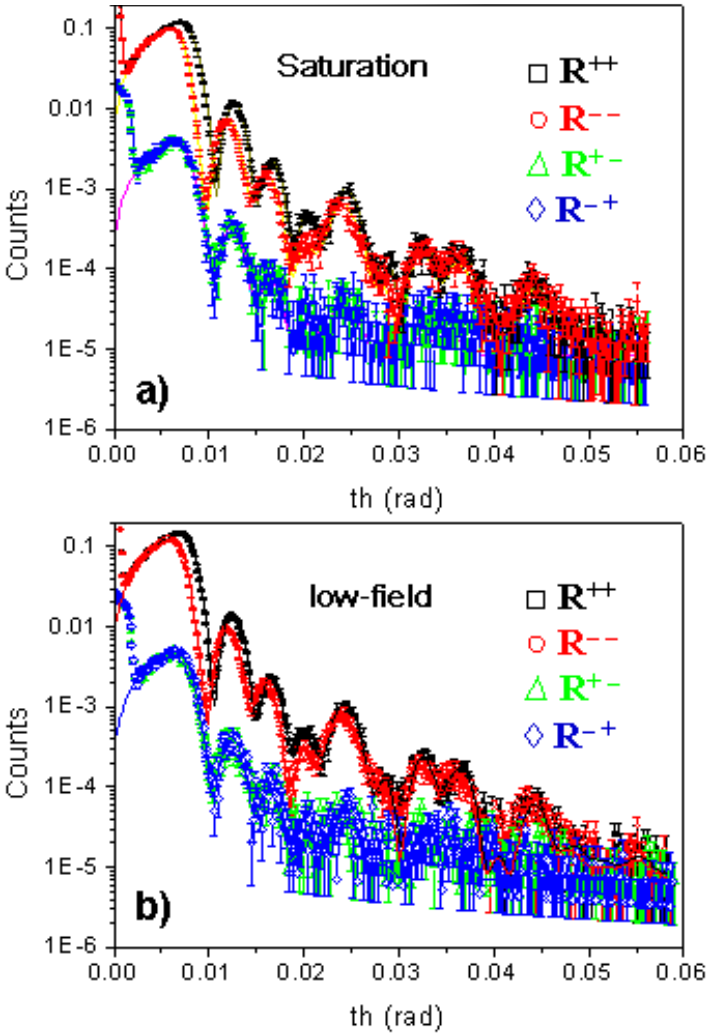

Figure 9. Polarized neutron experimental data (open symbols) and fittings (lines) versus angle 'th' from the CoCrPt20/Ni40 composite in (a) saturated and (b) low field (250 Oe) states. R^{++} (□ and black line), R^{--} (○ and red line), R^{+-} (△ and green line) and R^{-+} (◊ and blue line).

this hypothesis the magnetization profile through the depth of the bilayer was experimentally determined from PNR experiments. Two NSF, R^{++} and R^{--}, as well as two spin-flip (SF), R^{+-} and R^{-+}, reflectivity curves were recorded for a set of samples subjected to an external magnetic field up to 7 kOe. All four reflectivities were simultaneously fitted to a theoretical model from which a set of structural and magnetic parameters were determined.

The results for CoCrPt20/Ni40 measured both at saturation and at a low-field state (250 Oe) are presented in figure 9. In both sets of data, one can clearly see the splitting between reflection curves R^{++} and R^{--}. This splitting is caused by the difference in scattering length densities (SLD) $N_b + N_p$ and $N_b - N_p$ for alternative neutron spin projections onto the magnetization of the layers, with N_b and N_p the nuclear and magnetic SLD, respectively. SF reflection, in principle, probes deviations of magnetization from the external field direction. However, for data obtained both at saturation and close to remanence, the SF signal in figure 9 can be attributed

entirely to imperfection of the incident beam polarization (96.4%) and efficiency (95.3%) of the spin analysis. This means that no appreciable in-plane magnetization components perpendicular to the field guiding neutron polarization was detected in saturation, nor close to the remanent state.

Measurements in a saturating in-plane field of 7 kOe were used to firstly determine the basic sample parameters, e.g. thicknesses, SLDs, including magnetic, and interfacial roughness of the multilayer. They were reliably determined from the best fit of the PNR data to the theoretical model depicted in figure 9. It was, in particular, found that the FM layer thicknesses, 32.79 ± 0.06 nm for Ni and 18.45 ± 0.04 nm for CoCrPt layers, appreciably deviate from the nominal values of 40 and 20 nm, respectively, in the $3 \times 3\,\mathrm{cm}^2$ samples. Apart from this, the quality of the samples was rather good and the roughness of the interfaces does not exceed 1 nm. The nuclear SLD value for Ni layer was found close to its expected value $N_\mathrm{b} = (9.44 \pm 0.01) \times 10^{-6}\,\text{Å}^{-2}$, and the magnetic SLD $N_\mathrm{p} = (1.40 \pm 0.02) \times 10^{-6}\,\text{Å}^{-2}$, corresponding to magnetization [61] of $M_\mathrm{Ni}^\mathrm{PNR} = 482 \pm 7\,\mathrm{emu\,cm}^{-3}$, was consistent with the saturation magnetization for bulk nickel ($484.1\,\mathrm{emu\,cm}^{-3}$). At the same time, the average nuclear SLD of the CoCrPt layer was $N_\mathrm{b} = (2.88 \pm 0.06) \times 10^{-6}\,\text{Å}^{-2}$ with the magnetic SLD $N_\mathrm{p} = (1.06 \pm 0.05) \times 10^{-6}\,\text{Å}^{-2}$ corresponding to an in-plane magnetization of $M_\mathrm{CoCrPt}^\mathrm{PNR} \approx 360 \pm 20\,\mathrm{emu\,cm}^{-3}$. This value is larger than the CoCrPt magnetization obtained from our hysteresis loops ($M_\mathrm{SAT}^\mathrm{ave} \approx (330 \pm 20)\,\mathrm{emu\,cm}^{-3}$) and close to that from the literature ($\approx 350\,\mathrm{emu\,cm}^{-3}$) [36]. The origin of these discrepancies could be explained by the presence of amorphous interlayers between the CoCrPt and Ti seed layers, associated with the large lattice mismatch between the two elements and/or interdiffusion to form Co–Ti amorphous alloys [39, 62–65], and/or the existence of softer or even non-magnetic Cr-rich grain boundaries originated by Cr segregation to the grain boundaries of Co-rich grains [36].

Further measurements were performed in a low magnetic field of 250 Oe. Figure 9(b) shows that the splitting between NSF reflectivities, and hence the net magnetization of the sample, is appreciably reduced with respect to that in saturation (figure 9(a)). Such a reduction is expected from the VSM measurements and is due to the out of plane anisotropy of the CoCrPt. From the PNR data, the magnetic SLD of the Ni layer decreases to $(1.25 \pm 0.02) \times 10^{-6}\,\text{Å}^{-2}$ suggesting that $\approx$89% of the Ni magnetic moment remains aligned in plane. In contrast, the mean value of magnetic SLD of CoCrPt layer drops down to $(0.59 \pm 0.05) \times 10^{-6}\,\text{Å}^{-2}$ corresponding to $\approx$56% reduction in the net in-plane magnetization. Moreover, the best fit was achieved with gradients of magnetic SLD across the CoCrPt layer as illustrated in figure 9(b). This suggests a gradual decrease of in-plane magnetization of the CoCrPt layer from $\approx$65% at the interface with Ni layer down to only $\approx$20% of the saturation value at the interface with the substrate (figures 10(a) and (b)).

The progressive decay of the magnetization through the CoCrPt thickness indicates a non-uniform magnetization state in response to competition between the out of plane anisotropy, exchange coupling with the in-plane magnetized Ni, and demagnetization terms. Domain walls in CoCrPt thin films are expected to be narrow, e.g. 14 nm for a 20 nm thick film [66], the formation of a multidomain structure is facilitated even in thin films. A sketch of such a domain structure is given in figure 10(c), which includes triangular domains with out of plane magnetization and trapezoidal domains with in-plane magnetization coupled to the Ni, separated by 90° walls. Adjacent out-of-plane domains are separated by 180° walls. These arrangements provide partial flux closure while maintaining exchange coupling with the Ni.

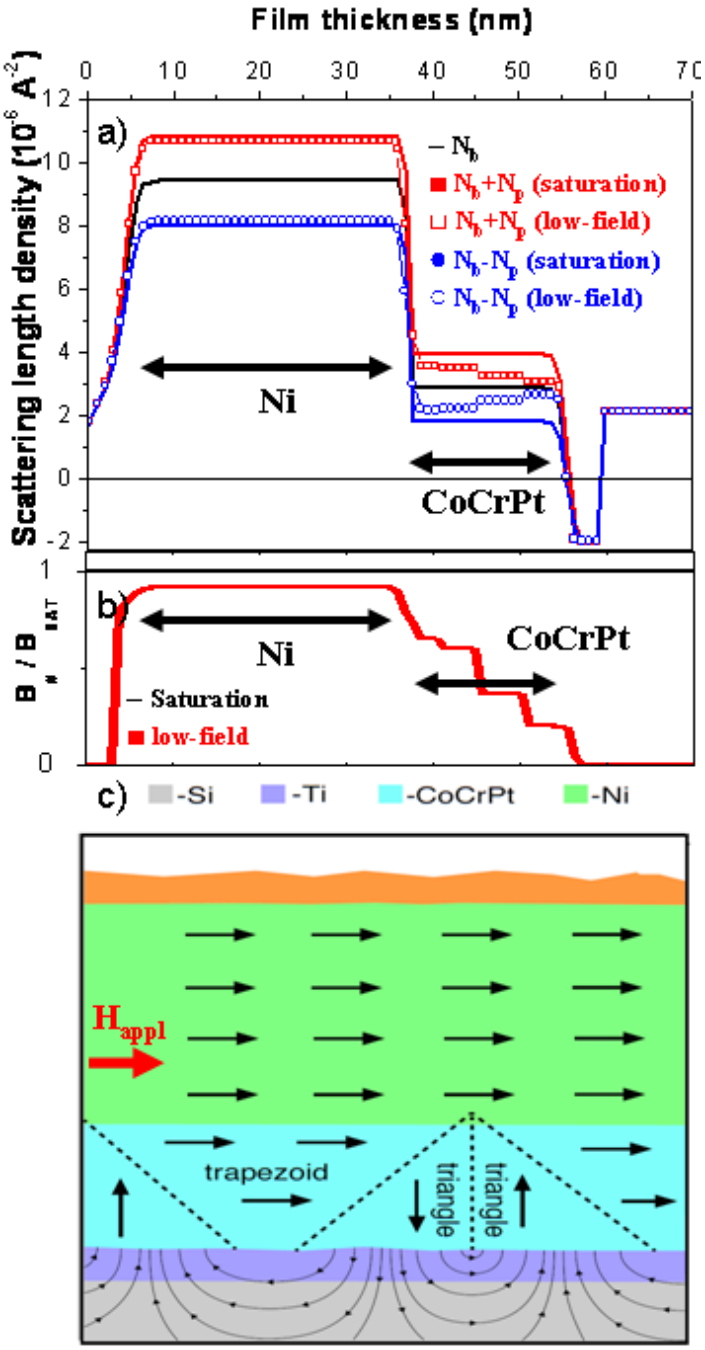

Figure 10. (a) Nuclear SLD (▬), (nuclear + magnetic) SLDs in saturation (■) and at low field, 250 Oe, (□) and (nuclear–magnetic) SLDs in saturation (●) and at 250 Oe (○) of the CoCrPt20/Ni40 composite. (b) Profile of the normalized in-plane magnetization at low field (■). (c) Proposed domain configuration in the interlayer between two films with perpendicular anisotropies. The magnetization direction is indicated by arrows.

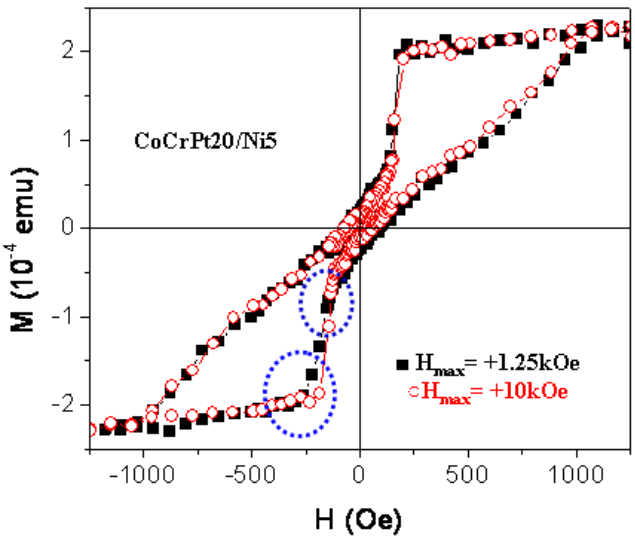

Figure 11. Out-of-plane hysteresis loops of CoCrPt20/Ni5 with +1.25 kOe (■) and +10 kOe (□) maximum applied field after saturating with +15 kOe. The blue circles point out the different return paths and the crossover of the hysteresis loops.

This model domain configuration is similar to those previously calculated for [Pt/Co] and NiFe bilayers by micromagnetic simulations [21] and experimentally determined for single FePd thin films with perpendicular anisotropy by using both circular dichroism in the x-ray resonant magnetic scattering [50] and grazing incidence small-angle neutron scattering [67] techniques. A precise determination of the parameters of the model is beyond the scope of the present work, but the model qualitatively explains the magnetization profile through the CoCrPt thin layer capped with thicker Ni layer observed by PNR, as well as illustrating the basic mechanism of the exchange bias effects experimentally observed for this bilayer system. The trapezoidal in-plane domains are stabilized by the out-of-plane domains, and interact with the Ni to provide a field-dependence pinning. The unidirectional orientation of the in-plane CoCrPt domains therefore explains the offset in the in-plane minor loops of the Ni. The interfacial exchange coupling, which is proportional to the interface area, can be significant even at remanence state, and complete reversal of the soft layer can only be achieved when all the domains in the hard layer are erased.

3.5. Exchange bias effects in CoCrPt/Ni composites in an out-of-plane field

Carrying out a similar process but with the external magnetic field applied perpendicular to the sample plane, an out-of-plane exchange bias effect between the two FM layers was obtained at room temperature. After the whole system was fully saturated (+15 kOe out-of-plane), shifts along the field axis (H_{EB}) (figure 11(a)) were obtained in the hysteresis loops when the maximum external field was large enough to saturate the hard phase. This effect was studied as a function of the soft and hard layer thicknesses. Figure 11 shows the out-of-plane hysteresis loops of CoCrPt20/Ni5 when the maximum applied fields were +1.25 and +10 kOe. The coercivity of the CoCrPt20/Ni5 minor loops was increased from 50 to 65 Oe when the maximum applied

fields were +10 and +1.25 kOe respectively. For CoCrPt20/Ni20 the coercivity of the minor loops was increased from 45 to 70 Oe when the maximum applied fields were +10and +2 kOe respectively. Also a positive bias field of 12 Oe was observed in the CoCrPt20/Ni5 loop with a maximum applied field of +1.25 kOe, and a bias field of 17 Oe for CoCrPt20/Ni20 at +2 kOe. No out-of-plane field-dependent shifts were obtained for CoCrPt10/NiY composites.

The origin of these features is believed to be different from the proposed interlayer domain configuration model responsible for in-plane bias effects. Davies *et al* [49] studied the magnetization reversal and FM domain formation of Co/Pt multilayer films by FORC analysis and transmission x-ray microscopy images, finding that the return path of some FORC curves (from negative to positive fields) cross over the major loop return path and the coercivity was increased. Magnetic imaging revealed that isolated residual domains, which were not fully reversed in the FORC curves, led to the crossover behavior by producing local stray fields that impeded subsequent domain growth, increasing the coercivity.

Based on this model, we propose that an out-of-plane field $H = -1.25$ kOe is insufficient to saturate the CoCrPt layer, leaving residual domains, as observed in our FORC analysis where irreversible features are observed between points H_A and vii in figure 5. This is indicated in the different return paths of the out-of-plane CoCrPt20/Ni5 hysteresis loops for +1.25 and +10 kOe maximum applied fields. The region of interest where the different return paths cross is shown in figure 11 and emphasized by circles. When the out-of-plane applied field approaches saturation, the number of residual domains decreases and a smaller net magnetization is observed with lower switching field and coercivity.

4. Summary

The magnetization reversal of exchange coupled CoCrPt/Ni composites was investigated using a combination of experimental techniques. The reversal shows a complex behavior due to the coupling between the layers and their orthogonal anisotropy axes (Ni: in plane, CoCrPt: out of plane easy axis). The major hysteresis loops of the bilayers show that the hard and soft layers are strongly coupled, so that the behavior of the composite is not a superposition of the hysteresis loops of each individual layer. The out-of-plane reversal process of the bilayer shows behavior characteristic of a film with perpendicular magnetic anisotropy and a multidomain structure. FORC results show two irreversible peaks (H_{Dp} and H_A) and a reversible region between them attributed to expansion of domains in the CoCrPt. The reversible field range increased with Ni thickness, from $\approx$1.05 to $\approx$1.25 kOe for CoCrPt20/Ni5 and CoCrPt20/Ni20 respectively. Fields well above the saturation field apparent from the hysteresis loops were required to completely saturate the CoCrPt phase and eliminate residual domains.

For both in- and out-of-plane fields, exchange bias effects were observed at room temperature which varied with layer thicknesses and field magnitude. The in-plane bias effect was attributed to the domain configuration in the CoCrPt at the interface with the Ni. The model is supported by the depth-dependence on CoCrPt magnetization according to PNR. In contrast, the out-of-plane bias effect was associated with residual domains in the CoCrPt which were not eliminated in the minor hysteresis loop. These exchange spring structures consisting of magnetic films with orthogonal anisotropies open the possibility to develop systems with controllable coercivity and loop asymmetry by varying the layer thicknesses and the magnetic history of the sample.

Acknowledgments

CAR and DN gratefully acknowledge the support of the National Science Foundation and the MIT-Spain/La Cambra de Barcelona Seed Fund. CR and DN thank the Ministerio de Economia y Competitividad for financial support (MAT2010-20798-C05-02).

References

[1] Richter H J 2007 *J. Phys. D: Appl. Phys.* **40** R149
[2] Judy J H 2005 *J. Magn. Magn. Mater.* **287** 16
[3] Weller D and Moser A 1999 *IEEE Trans. Magn.* **35** 4423
[4] Gao K Z and Bertram H N 2002 *IEEE Trans. Magn.* **38** 3675
[5] Wang J P, Zhou Y Y, Hee C H, Chong T C and Zheng Y F 2003 *IEEE Trans. Magn.* **39** 1930
[6] Ruigrok J J M, Coehoorn R, Cumpson S R and Kesteren H W 2000 *J. Appl. Phys.* **87** 5398
[7] Thiele J U, Maat S and Fullerton E E 2003 *Appl. Phys. Lett.* **82** 2859
[8] Maat S, Thiele J U and Fullerton E 2005 *Phys. Rev.* B **72** 214432
[9] Gruner M E, Hoffmann E and Entel P 2003 *Phys. Rev.* B **67** 064415
[10] Guslienko K Y, Chubykalo-Fesenko O, Mryasov O, Chantrell R and Weller D 2004 *Phys. Rev.* B **70** 104405
[11] Victora R H and Shen X 2005 *IEEE Trans. Magn.* **41** 537
[12] Suess D, Schrefl T, Dittrich R, Kirschner M, Dorfbauer F, Hrkac G and Fidler J 2005 *J. Magn. Magn. Mater.* **290** 551
[13] Suess D, Schrefl T, Fahler S, Kirschner M, Hrkac G, Dorfbauer F and Fidler J 2005 *Appl. Phys. Lett.* **87** 012504
[14] Dobin A Y and Richter H J 2006 *Appl. Phys. Lett.* **89** 062512
[15] Richter H J and Dobin A Y 2006 *J. Appl. Phys.* **99** 08Q905
[16] Asti G, Ghidini M, Pellicelli R, Pernechele C, Solzi M, Albertini F, Casoli F, Fabbrici S and Pareti L 2006 *Phys. Rev.* B **73** 094406
[17] Davies J E, Hellwig O, Fullerton E E, Jiang J S, Bader S D, Zimanyi G T and Liu K 2005 *Appl. Phys. Lett.* **86** 262503
[18] Pellicelli R, Pernechele C, Solzi M, Ghidini M, Casoli F and Albertini F 2008 *Phys. Rev.* B **78** 184434
[19] Goll D, Macke S and Kronmuller H 2008 *Physica* B **403** 338
[20] Wang F, Xu X, Liang Y, Zhang J and Wu H 2009 *Appl. Phys. Lett.* **95** 022516
[21] Bollero A, Buda-Prejbeanu L D, Baltz V, Sort J, Rodmacq B and Dieny B 2006 *Phys. Rev.* B **73** 144407
[22] Girt E, Dobin A Y, Valcu B, Richter H J, Wu X and Nolan T P 2007 *IEEE Trans. Magn.* **43** 2166
[23] Pandey K K M, Chen J S, Chow G M, Hu J F and Lim B C 2009 *J. Appl. Phys.* **105** 07B733
[24] Nogues J and Schuller I K 1999 *J. Magn. Magn. Mater.* **192** 203
[25] Berkowitz A E and Takano K 1999 *J. Magn. Magn. Mater.* 200 552
[26] Stamps R L 2000 *J. Phys. D: Appl. Phys.* **33** R247
[27] Kiwi M 2001 *J. Magn. Magn. Mater.* **234** 584
[28] Sort J, Popa A, Rodmacq B and Dieny B 2004 *Phys. Rev.* B **70** 174431
[29] Bollero A, Buda-Prejbeanu L D, Balt V, Rodmacq B and Dieny B 2006 *IEEE Trans. Magn.* **42** 2990
[30] Ploessl R, Chapman J N, Scheinfein M R, Blue J L, Mansuripur M and Hoffmann H 1993 *J. Appl. Phys.* **74** 7431
[31] Labrune M and Thiaville A 2001 *Eur. Phys. J.* B **23** 17
[32] Vukadinovic N, Ben Youssef J, Castel V and Labrune M 2009 *Phys. Rev.* B **79** 184405
[33] Bollero A, Baltz V, Buda-Prejbeanu L D, Rodmacq B and Dieny B 2011 *Phys. Rev.* B **84** 094423
[34] Baruth A and Adenwalla S 2008 *Phys. Rev.* B **78** 174407
[35] Nogues J, Stepanow S, Bollero A, Sort J, Dieny B, Nolting F and Gambardella P 2009 *Appl. Phys. Lett.* **95** 152515

[36] Inaba N, Uesaka Y and Futamoto M 2000 *IEEE Trans. Magn.* **36** 54
[37] Navas D, Nam C, Velazquez D and Ross C A 2010 *Phys. Rev.* B **81** 224439
[38] Oikawa K, Qin G W, Ikeshiji T, Kitakami O, Shimada Y, Ishida K and Fukamichi K 2001 *J. Magn. Magn. Mater.* **236** 220
[39] Sun C J, Chow G M, Wang J P, Soo E W and Je J H 2003 *J. Appl. Phys.* **93** 8725
[40] Davies J E, Hellwig O, Fullerton E E, Denbeaux G, Kortright J B and Liu K 2004 *Phys. Rev.* B **70** 224434
[41] Yin J, Zhang H, Hu F, Shen B and Pan L Q 2009 *J. Appl. Phys.* **106** 103901
[42] Cornejo D R, Peixoto T R F, Reboh S, Fichtner P F P, de Franco V C, Villas-Boas V and Missell F P 2010 *J. Magn. Magn. Mater.* **322** 827
[43] Panagiotopoulos I 2011 *J. Magn. Magn. Mater.* **323** 2148
[44] Zabel H, Theis-Bröhl K and Toperverg B 2007 *Handbook of Magnetism and Advanced Magnetic Materials* (*Novel Techniques for Characterization and Preparing Samples* vol 3) ed H Kronmuller and S Parkin (New York: Wiley) p 1237
[45] Alexandrakis V, Niarchos D, Wolff M and Panagiotopoulos I 2009 *J. Appl. Phys.* **105** 063908
[46] Kirby B J, Davies J E, Liu K, Watson S M, Zimanyi G T, Shull R D, Kienzle P A and Borchers J A 2010 *Phys. Rev.* B **81** 100405
[47] Hellwig O, Berger A and Fullerton E 2007 *Phys. Rev.* B **75** 134416
[48] Dürr H *et al* 2009 *IEEE Trans. Magn.* **45** 15
[49] Davies J E, Hellwig O, Fullerton E E, Winklhofer M, Shull R D and Liu K 2009 *Appl. Phys. Lett.* **95** 022505
[50] Dürr H A, Dudzik E, Dhesil S S, Goedkoop J B, van der Laan G, Belakhovsky M, Mocuta C, Marty A and Samson Y 1999 *Science* **284** 2166
[51] Ilievski F, Perkinson J C and Ross C A 2007 *J. Appl. Phys.* **101** 09D116
[52] Ilievski F, Ross C A and Vancso G J 2008 *J. Appl. Phys.* **103** 07C520
[53] Clime L, Stancu A, Ciureanu P and Yelon A 2004 *J. Optoelectron. Adv. Mater.* **6** 1005
[54] Mayergoyz I D 1991 *Mathematical Models of Hysteresis* (New York: Springer)
[55] Sun H Y, Hu J, Su Z F, Xu J L and Feng S Z 2006 *IEEE Trans. Magn.* **42** 1782
[56] Skomski R and Coey J M D 1993 *Phys. Rev.* B **48** 15812
[57] Suess D 2007 *J. Magn. Magn. Mater.* **308** 183
[58] Kooy C and Enz U 1960 *Philips Res. Rep.* **15** 7
[59] Hubert A and Schafer R 1998 *Magnetic Domains: The Analysis of Magnetic Microstructures* (New York: Springer)
[60] Gong W J, Liu W, Liu X H, Guo S, Feng J N, Li B and Zhang Z D 2011 *J. Appl. Phys.* **109** 043906
[61] Theis-Brohl K, Wolff M, Ennen I, Dewhurst C D, Hutten A and Toperverg B P 2008 *Phys. Rev.* B **78** 134426
[62] Lee I S, Ryu H, Lee H J and Lee T D 1999 *J. Appl. Phys.* **85** 6133
[63] Platt C L, Wierman K W, Svedberg E B, Klemmer T J, Howard J K and Smith D J 2002 *J. Magn. Magn. Mater.* **247** 153
[64] Saito S, Hoshi F and Takahashi M 2002 *J. Appl. Phys.* **91** 8028
[65] Saito S, Hasegawa D, Hoshi F, Djayaprawira D D and Takahashi M 2002 *Appl. Phys. Lett.* **80** 811
[66] Navas D, Ilievski F and Ross C A 2009 *J. Appl. Phys.* **105** 113921
[67] Pannetier M, Ott F, Fermon C and Samson Y 2003 *Physica* B **335** 54